J Mater Sci (2009) 44:1063–1068
DOI 10.1007/s10853-008-3158-0

Formation of feathery grains with the application of a static magnetic field during direct chill casting of Al-9.8wt%Zn alloy

Lei Li · Yudong Zhang · Claude Esling · Zhihao Zhao · Yubo Zuo · Haitao Zhang · Jianzhong Cui

Received: 1 September 2008 / Accepted: 3 December 2008 / Published online: 14 January 2009

Abstract Effect of a 0.2-T static magnetic field on the microstructure of a direct chill cast Al-9.8wt%Zn alloy slab was investigated. The static magnetic field transferred the microstructure from a mixture of equiaxed and columnar grains with the primary trunks growing in <100> directions to twinned lamellar feathery grains with the primary and secondary arms growing in <110> directions. The application of the static magnetic field results in the reduction of the heat discharge and solute mixing capacity through a damping effect on convection and thus a delay of the melt transformation to solid and a request to reduce the liquid/solid interface energy through reducing the interface area due to the loss of undercooling. The delay and the request account for the growth direction change and the formation of lamellas. The difference between the Al and Zn atomic radii and the related incoming flow facilitate the formation of the twins.

L. Li · Y. Zhang · Z. Zhao · Y. Zuo · H. Zhang · J. Cui
Key Laboratory of Electromagnetic Processing of Materials, Ministry of Education, Northeastern University, Shenyang 110004, People's Republic of China
e-mail: li_lei@live.com

Y. Zhang
e-mail: yudong.zhang@univ-metz.fr

Z. Zhao
e-mail: zzh@epm.neu.edu.cn

Y. Zuo
e-mail: zuoyubo@epm.neu.edu.cn

H. Zhang
e-mail: haitao_zhang@epm.neu.edu.cn

J. Cui
e-mail: jzcui@epm.neu.edu.cn

L. Li · Y. Zhang · C. Esling (✉)
LETAM, CNRS-UMR 7078, University of Metz, Ile du Saulcy, 57045 Metz, France
e-mail: claude.esling@univ-metz.fr

Introduction

Feathery grains, as specific and undesirable microstructure, are occasionally spotted in aluminum alloys under certain conditions during direct chill (DC) casting. Several efforts have been made to reveal the crystallographic characteristics and the formation conditions of this microstructure. It was found [1, 2] that they are the result of a <110> dendrite growth with each primary trunk split by a twin plane, showing a transition of the growth direction from the usual <100> to <110>. The twin plane is associated with stacking faults which are favored by a strong shearing rate related to convection, while the transition of the growth direction is induced by solute additions and/or solidification conditions (thermal gradient, growth rate, and melt convection). It was further clarified that under forced flow conditions the feathery growth is an intermediate case between equiaxed and columnar growth and similar to the growth of <100> regular dendrites with the competitive branching–twinning mechanisms [3]. Despite many years of investigations [1–6], the formation mechanism of feathery grains is still not clearly understood and further investigation is required.

Recently, the application of electromagnetic fields to material processing, in the field of solid-state phase transformation [7–11] and solidification [12–17], has been regarded as a new topic. As a unique means, introducing an external static magnetic field to a DC casting may offer a new chance to gain new insights into the formation mechanism of the feathery grains. Since a static magnetic

field can damp the convection in the bulk liquid which has a great influence on heat and solute transfer, the microstructure will probably be changed accordingly. Based on this, an Al-9.8wt%Zn slab was cast without and with a static magnetic and the formation mechanism of feathery grains was studied in this present work.

Experiment section

An Al-9.8wt%Zn slab with dimensions of 50 × 100 × 1000 mm was produced by a DC casting process. The casting configuration is schematically illustrated in Fig. 1a. The pouring temperature was 720 °C, and the casting speed V_0 was 3 mm/s. The melt was introduced to the mold by a horizontal inlet through the short-dimensioned side of the hot top. The first half of the slab was cast without switching on a magnetic field, while the second half was cast under a horizontal static magnetic field B_0 with a nominal value of 0.2 T. The field was imposed perpendicularly to the casting direction V_0, as shown in Fig. 1a. Two transverse slices with dimensions of 50 × 100 × 20 mm to the casting direction V_0 were cut out from the respective non-field cast and field cast halves for macrostructure observation. After macrostructure observation, specimens of dimensions 5 × 5 × 5 mm were further cut out from the slices for microstructural analysis. The relative positions between the specimen, slice and slab are schematically shown in Fig. 1b. The microstructure observation was performed in the transverse section to the casting direction V_0 (Surface 1), and in the two longitudinal sections, one parallel to the field direction B_0 (Surface 2) and the other nearly perpendicular to B_0 (Surface 3) as indicated in Fig. 1b to obtain the 3D microstructural information.

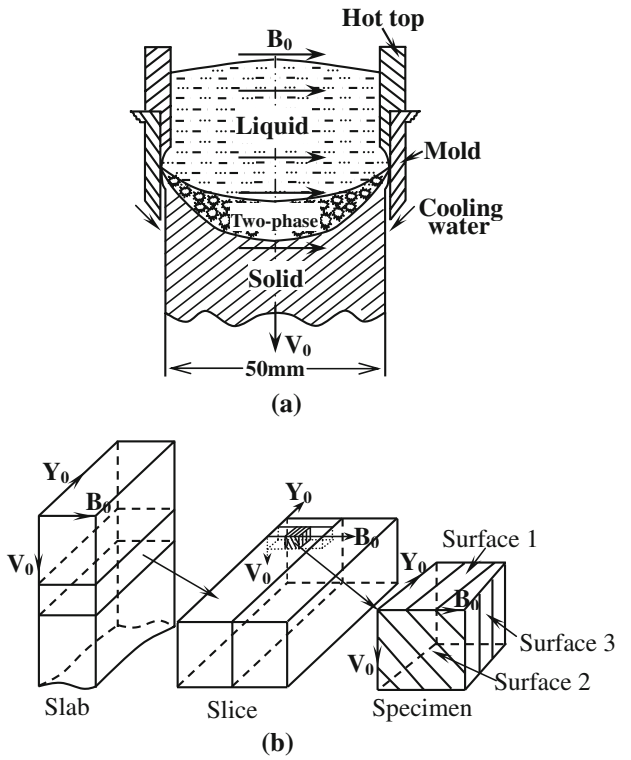

Fig. 1 Schematic diagram of **a** the DC casting configuration and **b** the relative positions of the slice and the specimen in the cast slab. B_0, Y_0, and V_0 are the horizontal static magnetic field, pouring direction and casting direction, respectively

The macrostructures of the two slices were etched with NaOH (100 g/L) reagent for 8 min after mechanical polishing and then washed with HNO_3 (20%) reagent and taken with an OLMPUS C8080WZ camera, while the microstructures were etched with Keller's reagent (2 mL HF (48%), 3 mL HCl (concentrated), 5 mL HNO_3 (concentrated), 190 mL H_2O) for a few seconds and observed using an OLYMPUS BX61 optical microscope. The crystallographic orientations of the microstructural constituents in the non-field and field-treated specimens were measured and analyzed by EBSD technique attached to a JOEL 6500F SEM, equipped with Channel 5 software (a software package developed by HKL Technology A/S for measuring and analyzing EBSD (back scattered electron diffraction pattern) data to obtain microstructural and crystallographic information of the measured materials) after an electrolytic polishing (700 mL ethanol, 120 mL distilled water, 100 mL 2-butoxyethanol, and 80 mL perchloric acid 40 V, 5 s). The EBSD mapping was performed with a step size of 2 μm.

Results

Figure 2 shows the cross-sectional macrostructures of the non-field and field cast parts of the slab. It can be observed that without the magnetic field the grains are mainly equiaxed, while with the field the grains are lamellar.

The EBSD orientation micrographs from the cross section and the longitudinal section (Surfaces 1 and 2 in Fig. 1b) of the non-field and field cast specimens are shown in Fig. 3. From the two perpendicular sections, the 3D image of the microstructure can be figured out. It is found that without the field (Fig. 3a, b), the microstructure consists of equiaxed and columnar grains, while with the field, the microstructure (Fig. 3c, d) is mostly composed of feather-like lamellas that are usually called "feathery crystals." The red lines in Fig. 3c and d display the CSL Σ3 boundaries (we remind that CSL is the abbreviation of coincident site lattice in which the orientations of the two neigboring grains allow some lattice points of one grain coincide exactly with some lattice points of the other grain, see e.g. [18]). This boundary indicates that in cubic system the two neighboring crystals are related to each other by a 60° rotation around the common <111> axis. It has been

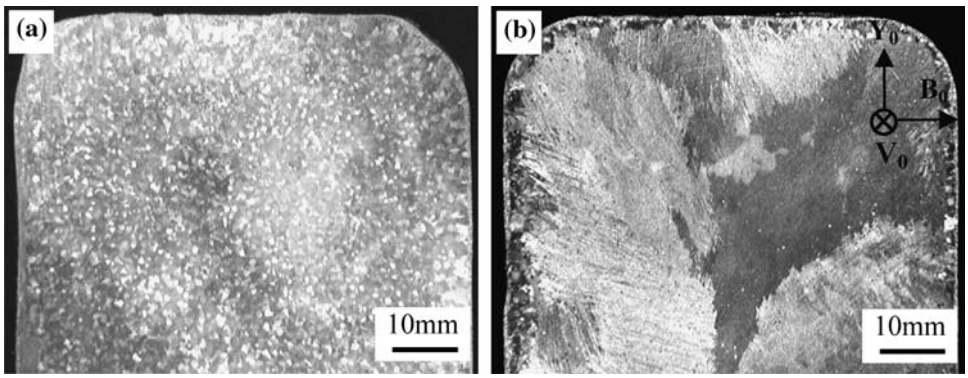

Fig. 2 Macrostructures of the cross sections (to the casting direction V_0) of specimens cast without (**a**) and with (**b**) a 0.2-T static magnetic field

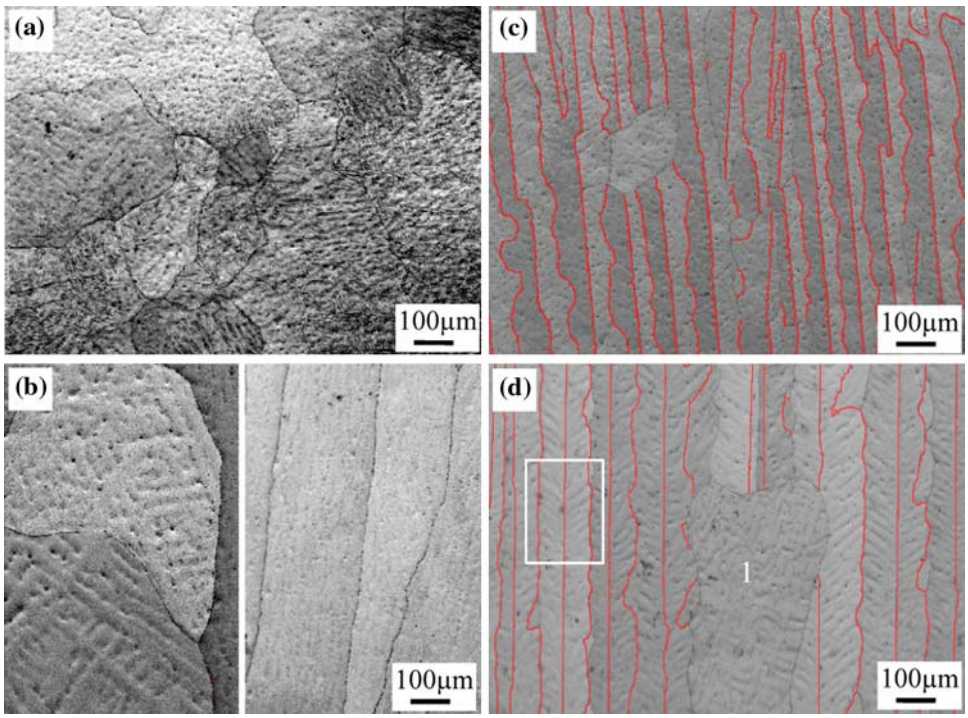

Fig. 3 EBSD orientation micrographs of the cross section and the longitudinal section (Surfaces 1 and 2 in Fig. 1b) of the non-field and field cast specimens. **a** Surface 1 and **b** Surface 2 of the non-field cast specimen; **c** Surface 1 and **d** Surface 2 of the field cast specimen. Straight and wavy lines in Fig. 3c and d are Σ3 boundaries. The microstructure enclosed in the white frame will be further analyzed in Fig. 4

well clarified that in FCC structures this orientation relationship defines the twin relation between the two crystals [19]. The twinning plane is {111} and twinning direction is <11−2>. Figure 3c and d clearly reveal the feathery character of the microstructure [1] obtained by magnetic field casting. It is composed of thin lamellas, separated by straight and wavy boundaries, most of which are Σ3 boundaries. The straight Σ3 boundaries represent the coherent twin boundaries, while the wavy boundaries represent the incoherent twin boundaries. Columnar grains are occasionally spotted, but their growth is often suppressed by the feathery grains (i.e., 1 in Fig. 3d). Moreover, no Σ3 boundaries are found in Fig. 3a and b.

The grains of the non-field and field cast specimens differ from each other also in crystallographic growth direction. Figure 4a displays the <100> pole figure of the columnar grains in the non-field cast specimen shown in the right part of Fig. 3b. It can be observed that all grains share one <100> pole that is enclosed in the black square in Fig. 4a. The corresponding <100> direction is closely parallel to the casting direction V, indicating that the principal growth direction of the columnar grains is <100>. Figure 4b shows the <110> pole figure of the feathery grains enclosed in the white rectangle in Fig. 3d and the zoomed micrograph. The black poles are from the left part of the feathery grains and the gray ones in the circles from the twinned right part. The poles in the rectangles are common for both parts. The micrograph well reveals one kind of secondary arms of the twinned feathery grain. From the contour ($O'C'$ and $O'D'$ in the micrograph of Fig. 4b) of the secondary arms outlined by the dark contrast resulting from the solute segregation, it can be observed that they go continuously from the straight twinning boundary to the wavy boundaries that separate the adjacent feathery

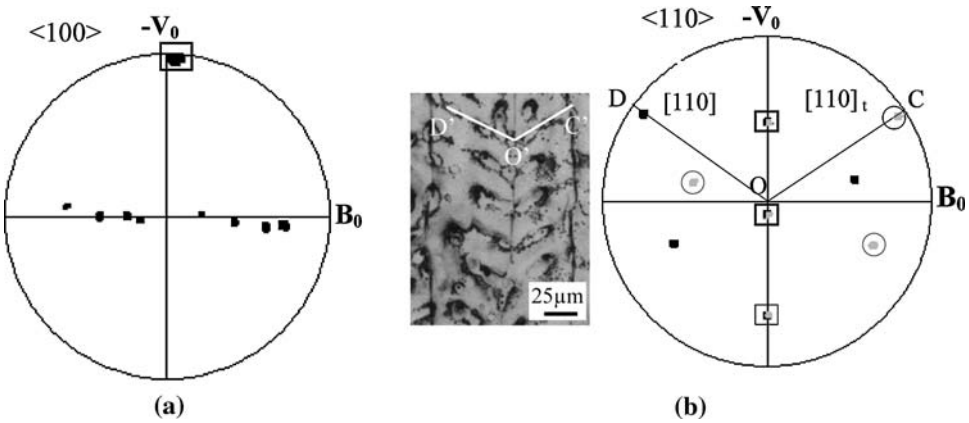

Fig. 4 **a** <100> Pole figure corresponding to the right part of the microstructure in Fig. 3b. **b** <110> Pole figure of the corresponding feathery grains enclosed in the white rectangle in Fig. 3d and the zoomed micrograph

crystals, evidencing that the sectioning plane is parallel to the main axis of these secondary arms. The projection lines of the [110] (Line OD) and $[110]_t$ (Line OC) in Fig. 4b are very close to the true [110] and $[110]_t$ crystal lines as their poles are close to the outer circle of the pole figure (The index "t" refers to the twinned part as opposed to the matrix). In addition, OC and OD are, respectively, parallel to the secondary arm traces O′C′ and O′D′ in the micrograph. This indicates that these secondary arms grow along <110> directions.

To find out the primary trunk and other possible secondary arms, and their growth directions, the microstructure on the (111) plane (the twinning plane, corresponding to Surface 3 in Fig. 1b) was etched out and is shown in Fig. 5. The related <110> pole figure is also displayed in the same figure. The micrograph in Fig. 5 clearly indicates the configuration of the primary trunk and the secondary arms that are distributed on both sides of the primary trunk. Following the same analyzing principles described above, it is found that the growth directions of the primary trunk (O′A′) and those of the two secondary arms (O′C′ and O′B′) correspond to the poles A, B, and C in the <110> pole figure. Thus, their growth directions can be determined as <110>.

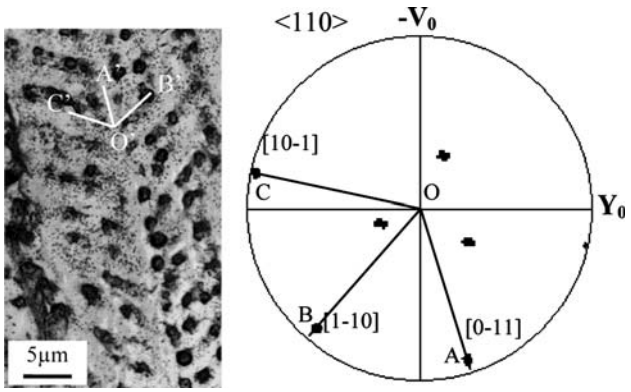

Fig. 5 Microstructure on the {111} twinning plane (corresponding to Surface 3 in Fig. 1b and the corresponding <110> pole figure

It should be noted that each of these secondary arms should possess a twinned counterpart with respect to the (111) twinning plane.

Discussion

For small slab casting, as in the case of the present study, columnar grains are generally expected due to the approximate one-dimensional heat transfer in normal continuous casting condition (without a magnetic field) except those equiaxed grains forming in the peripheral region near the mold surface. However, dendrite fragmentation and subsequent crystal multiplication during solidification can happen due to convection [20, 21]. When a secondary branch of a columnar dendrite initially forms, an increase in the local temperature or shearing force due to convection can detach it from the dendrite. These fragments act as seeds for the equiaxed grains if the thermal and compositional conditions are appropriate. In this present experiment, this convection in the bulk liquid can be induced both by the temperature and solute concentration difference (natural convection), and mold filling (forced convection). Moreover, equiaxed grains can also probably grow from predendritic crystals which are formed during pouring at or near the mold and brought to the bulk by convection with some surviving. Thus, equiaxed and columnar grains coexist in the non-field cast sample (Fig. 3a, b).

When a static magnetic field is applied to the second half of the slab, the convection condition in the bulk liquid is modified. It is known that when the electroconducting melt crosses a static magnetic field B, an electric current J in a direction perpendicular to the fluid velocity V and the magnetic field B will be induced. The interaction of this current J with the applied magnetic field B leads to a Lorentz force $J \times B$ that damps the melt motion [22–24]. The effectiveness of the magnetic field in damping the convection is generally weighed by the value of Hartman number $\mu BL\sqrt{\sigma/\eta_0}$ [25], where μ is the relative magnetic

permeability ($\mu = 1$) [26], B is the magnetic field strength (0.2 T), L is a characteristic length of the system, σ is electrical conductivity, and η_0 is viscosity of the melt. Here, half width of the short-dimensioned side of the mold (0.025 m) is taken as the characteristic length of the system [26]. At 727 °C (close to the pouring temperature), the respective electrical conductivities of the pure aluminum and the aluminum with 70–80% zinc are $4 \times 10^6\ \Omega^{-1}\ m^{-1}$ and $2.63 \times 10^6\ \Omega^{-1}\ m^{-1}$, while the respective viscosities of the pure aluminum and the aluminum with 30% zinc are 1.718×10^{-3} Pa·s [27] and 2.23×10^{-3} Pa·s [28]. It is known that the electrical conductivity of the aluminum lineally decreases with the increase of zinc content, while the viscosity is just the opposite, i.e., it lineally increases with the increase of zinc in proportion [29]. In this present work, we can easily interpolate the respective electrical conductivity σ and the viscosity η for the used alloy. They are $3.82 \times 10^6\ \Omega^{-1}\ m^{-1}$ and 1.89×10^{-3} Pa. The Hartman number for the present growth conditions is 224.8. It has been proved that the convection was completely damped with a Hartman number of 54 by a vertical magnetic field during Czochralski growth of molten gallium [30]. Therefore, with such a large Hartman number 224.8 in the present conditions, it can be indicated that the melt motion in the direction of Y_0 and V_0 is effectively weakened by the field. In other words, the effective viscosity of the melt (magnetic viscosity induced by the magnetic field and the viscosity in its own) is remarkably enhanced by the field. Here, it should be mentioned that the magnetic viscosity plays a leading role in the present study as the Hartman number is much larger than 1($224.8 \gg 1$).

It is well known that the convection heat and mass transfer ability decreases with the increase of viscosity. Therefore, the direct influence of the damping effect is that it reduces the heat discharge into the mold and the solid and lowers the solute mixing capacity of the melt. Thus, the superheat evacuation of the melt in the bulk liquid decreases and the latent heat generated by solidification and the solute atoms with low melting point—Zn in the present case—concentrates at the solid/liquid interface. The concentrated latent heat raises the solid front temperature and the segregated solute atoms lower the melting point of the melt at the same front. Both result in the decrease of the undercooling degree, as the undercooling degree is the temperature difference between the melting point and the real solidification temperature, i.e., the solid front temperature. It should also be noted that the solidification of the first half of the slab provides the same contribution to latent heat and solute enrichment and further decreases the undercooling degree at the solid front. The reduction of the superheat evacuation delays the melt transformation from the liquid to solid [31] and the loss of undercooling requests to lower the solid/liquid macro interfacial energy according to the thermodynamic theory. The solidification path with lower interfacial energy is then triggered. This may account for the growth direction change from <100> (columnar grain) to <110> (feathery grain) and result in the morphology change (from mixed columnar and equiaxed grains to lamellar crystals).

It has been proved that in most metal systems with dendritic growth character, the solid/liquid interface is rough and exposes a lot of sides for the attachment of atoms from the liquid [32]. In the low undercooling condition, reducing interfacial area means lowering its microscopic roughness. A more flat interface would be an ideal configuration. The <110> primary trunk surrounded by symmetrically distributed up-flow secondary <110> arms could offer a microscopically flatter solid/liquid front, as shown in Fig. 6b, when compared with the solid/liquid front with mixed equiaxed and columnar grains as in the case of the first half of slab cast without a magnetic field. The arrangement of the parallel primary trunks with the same surrounding secondary arms in one direction forms one-twinned feathery lamella and the packing of the identical lamellas in the perpendicular direction forms a cluster of feathery crystals. This would offer a large stretch of low roughness solid/liquid interface. In this way, large clusters of the feathery lamellas appear.

Furthermore, the effective damping of convection by the magnetic field decreases the detachment of fragments from the secondary arms that act as seeds for equiaxed grains and usually block the growth of columnar grains. Thus, the field provides a favorable environment and promotes the growth of feathery grains.

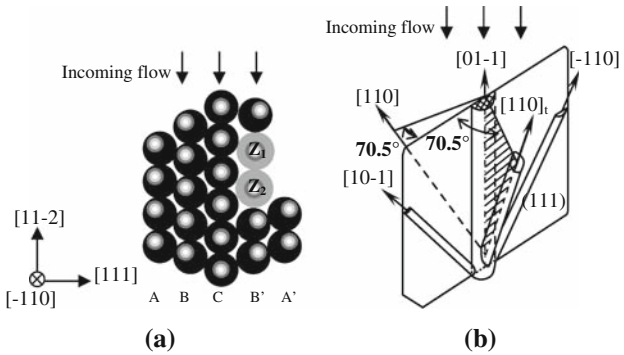

Fig. 6 Schematic illustration of **a** (111) Stacking fault induced by the atomic radius difference between aluminum and zinc and the incoming flow; **b** the symmetrical distribution of the secondary arms around the primary trunk in the feathery crystal. In (**a**), it is a projection of atoms on (−110) plane. Z_1 and Z_2 are zinc atoms and the others are aluminum atoms. The aluminum atoms in B′ layer below Z_1 and Z_2 are pushed down and assume a mirror reflection position of the atoms in B with respect to the layer C

Conclusions

The solidification microstructure of the Al-9.8wt%Zn alloy changes from the equiaxed and columnar grains to the lamellar feathery grains accompanied by the crystallographic growth direction change from <100> to <110> after the application of a static magnetic field. By damping convection, the field decreases the heat discharge and solute mixing capacity and thus results in the reduction of the superheat evacuation of the melt in the bulk liquid and the loss of undercooling degree at the liquid/solid front. The reduction of the superheat evacuation changes the crystalline growth direction of the solidified dendrite from the normal non-close packed <100> to the close packed <110> to accommodate the delay of the melt transformation from the liquid to solid. With the change of the growth direction, the segregation of Zn atoms having different atomic radius from Al at the solid front and the related incoming flow give rise to the formation of twinned crystals. Moreover, the request to reduce the solid/liquid interfacial energy related to the loss of undercooling through reducing microscopic interfacial roughness contributes to the formation of lamellar feathery crystals.

Acknowledgements This study was financially supported by the Key Fundamental Program of China [(973), Grant No. 2005CB623707], the Cultivation Fund of 111 (Grant No. 704015), the national Natural Science Foundation (Grant No. 50674030) and the CNRS-PICS (No. 4164). The first author also gratefully acknowledges the CHINA SCHOLARSHIP COUNCIL for the Chinese-French cotutelle Ph.D. Grant.

References

1. Henry S, Jarry P, Rappaz M (1998) Metall Mater Trans A 29:2807
2. Henry S, Gruen G-U, Rappaz M (2004) Metall Mater Trans A 35:2495
3. Turchin AN, Zuijderwijk M, Pool J et al (2007) Acta Mater 55:3795
4. Eady JA, Hogan LM (1974) J Cryst Growth 23:129
5. Granger DA, Liu J (1983) JOM 35:54
6. Anada H, Tada S, Koshimoto K, Hori S (1991) J Jpn Inst Light Met 41:497
7. Sheikh-Ali AD, Molodov DA, Garmestani H (2006) Rev Adv Mater Sci 11:167
8. Gao MC, Bennett TA, Rollett AD, Laughlin DE (2006) J Phys D Appl Phys 39:2890
9. Beaugnon E, Rivoirard S, Garcin T, Bouaziz O (2006) In: Proceedings of the 5th international symposium on electromagnetic processing of materials, Sendai, Japan, p 604
10. Rivoirard S, Garcin T, Gaucherand F, Bouaziz O, Beaugnon E (2006) J Phys Conf Ser 51:541
11. Nakamichi S, Tsurekawa S, Morizono Y, Watanabe T, Nishida M, Chiba A (2005) J Mater Sci 40:3191. doi:10.1007/s10853-005-2683-3
12. Li X, Fautrelle Y, Ren ZM (2007) J Cryst Growth 306:187
13. Li X, Fautrelle Y, Ren ZM (2007) Acta Mater 55:5333
14. Wang Q, Wang CJ, Liu T, Wang K, He JC (2007) J Mater Sci 42(24):10000. doi:10.1007/s10853-007-2050-7
15. Ban CY, Cui JZ, Han Y, Ba QX (2006) J Mater Sci 41(10):3113. doi:10.1007/s10853-006-5243-6
16. Cramer A, Eckert S, Galindo V, Gerbeth G, Willers B, Witke W (2004) J Mater Sci 39(24):7285. doi:10.1023/B:JMSC.0000048743.43663.e9
17. Yang S, Liu WJ, Jia J (2001) J Mater Sci 36(22):5351. doi:10.1023/A:1012467817033
18. Zuo L, Watanabe T, Esling C (1994) Z Metallkde 85:554
19. Rollett AD (2002) In: Proceedings of the 8th international conference on aluminum and its alloys (ICAA8)
20. Hunt JD, Jackson KA (1967) Trans Met Soc AIME 239:864
21. O'Hara S, Tiller WA (1967) Trans Metall Soc AIME 239:497
22. Lehmann P, Moreau R, Camel D, Bolcato R (1998) Acta Mater 46:4067
23. Gillon P (2000) Mater Sci Eng A 287:146
24. Tewari SN, Shah R, Song H (1994) Metall Mater Trans A 25:1535
25. Carruthers JR (1977) In: Wilcox WR, Lefever RA (eds) Preparation and properties of solid state materials, vol 3. Marcel Dekker, New York, p 1
26. International Handbook Committee (1961) Metals handbook. ASM, Metals Park, OH, vol 1, p 1064
27. Assael MJ, Kakosimos K, Banish RM, Brillo J, Egry I, Brooks R, Quested PN, Mills KC, Nagashima A, Sato Y, Wakeham WA (2006) J Phys Chem Ref Data 35:299
28. Mondolfo LF (1976) Aluminum alloys: structure and properties. Butterworths, London
29. Hunt JCR (1965) J Fluid Mech 21:577
30. Szabo G, Juhaz Z, Paitz J, Poltl J (1986) J Cryst Growth 78:558
31. Haxhimali T, Karma A, Gonzales F, Rappaz M (2006) Nat Mater 5:660
32. Cantor B, Vogel A (1977) J Cryst Growth 41:109